applied sciences

MDPI

Article

Monitoring Landslide Deformation in the Xiluodu Reservoir Area Using Combined Ascending and Descending Orbit Time-Series InSAR Technology

Xiaodong Wang [1], Yunchang Liang [1,*], Fuchu Dai [2] and Zihan Wang [1]

[1] College of Geosciences and Engineering, North China University of Water Resources and Electric Power, Zhengzhou 450046, China; wangxiaodong@ncwu.edu.cn (X.W.); wzh85867@163.com (Z.W.)
[2] College of Architecture and Civil Engineering, Beijing University of Technology, Beijing 100124, China; fc_dai@126.com
* Correspondence: 19503822296@163.com; Tel.: +86-19503822296

Abstract

The process of reservoir impoundment poses a significant threat to the stability of reservoir bank slopes, potentially triggering new landslides or reactivating ancient ones. Consequently, long-term and stable monitoring of surface deformation in reservoir areas is essential for ensuring safe reservoir operation. SBAS-InSAR technology—characterized by its high precision, multi-temporal capability, and wide spatial coverage—offers an effective means of comprehensively characterizing landslide deformation in such environments. In this study, SBAS-InSAR is applied to monitor landslides in the Xiluodu Reservoir area using Sentinel-1A imagery. Ascending and descending orbit data are jointly inverted to reconstruct the two-dimensional (2D) surface deformation time series. The deformation patterns and their spatiotemporal evolution are analyzed in conjunction with remote sensing imagery, topographic and geological data, and reservoir water level fluctuations. The integrated analysis identifies 10 and 12 significant deformation zones in the vertical and east–west directions, respectively—demonstrating improved detection accuracy compared to single-orbit approaches. Two representative landslides, the Mixiluo and Huanghua landslides, are selected for detailed investigation. Their toe deformation exhibits a pronounced response to both rainfall and reservoir water level variations. These findings provide valuable reference data and technical support for the early identification of reservoir bank landslides and the safe operation of reservoirs in this and similar engineering contexts.

Keywords: SBAS-InSAR; landslide monitoring; ascending and descending orbits; reservoir area; deformation characteristics

check for updates

Academic Editor: Tiago Filipe da Silva Miranda

Received: 30 September 2025
Revised: 17 October 2025
Accepted: 24 October 2025
Published: 1 November 2025

Citation: Wang, X.; Liang, Y.; Dai, F.; Wang, Z. Monitoring Landslide Deformation in the Xiluodu Reservoir Area Using Combined Ascending and Descending Orbit Time-Series InSAR Technology. *Appl. Sci.* **2025**, *15*, 11698. https://doi.org/10.3390/app152111698

Copyright: © 2025 by the authors. Licensee MDPI, Basel, Switzerland. This article is an open access article distributed under the terms and conditions of the Creative Commons Attribution (CC BY) license (https://creativecommons.org/licenses/by/4.0/).

1. Introduction

As a large-scale hydraulic hub on the lower reaches of the Jinsha River, the Xiluodu Hydropower Station plays an irreplaceable role in flood control, power generation, and sediment retention. However, the reservoir impoundment operation has altered the original geological and hydrogeological conditions of the reservoir area and its surrounding regions. This poses significant challenges to the stability of the reservoir banks [1,2]. The infiltration effect of reservoir water significantly reduces the shear strength of the rock and soil mass along the banks. Frequent fluctuations in reservoir water levels cause changes in the dynamic seepage field, which increases pore water pressure within the slope body and thereby weakens the effective stress. These factors collectively exacerbate the risk

of slope deformation and instability [3–5]. In the event of a large-scale Landslide, the lives and property of residents in the reservoir area may be directly threatened. Landslide debris entering the reservoir area may also generate surge waves that impact the dam structure, posing a serious threat to the safe operation of the reservoir. For high-mountain canyon reservoir areas such as the Xiluodu Reservoir Area, characterized by significant topographic relief, dense vegetation, and limited accessibility, conducting high-precision, full-coverage, long-term surface deformation surveillance has become an urgent requirement. It is essential for scientifically assessing reservoir bank stability, providing early warnings of potential hazards, and optimizing reservoir scheduling strategies to ensure the long-term safe operation of the reservoir.

Traditional Landslide surveillance methods, such as leveling and Global Positioning System (GPS) measurement, are simple to operate and relatively accurate. However, they face limitations in wide-ranging and topographically complex areas, such as the Xiluodu Reservoir Area. These limitations include restricted surveillance coverage, high costs, and difficulty in achieving real-time monitoring [6,7]. In recent years, Interferometric Synthetic Aperture Radar (InSAR) technology has been widely applied because it can perform large-scale, high-precision surface deformation surveillance [8]. The Small Baseline Subset Interferometric Synthetic Aperture Radar (SBAS-InSAR) technique mitigates the issues caused by spatiotemporal decorrelation by processing Multi-temporal SAR images. This significantly enhances surveillance capabilities in areas with unstable interferometric conditions, such as mountainous regions. Currently, SBAS-InSAR Technology is widely used in the deformation surveillance of reservoir area Landslides [9–11]. For example, Feng Wenkai et al. (2020) conducted surface deformation surveillance of the Woda Village Landslide in the Jinsha River Basin. They analyzed the Deformation Characteristics of the reactivated zone of the Landslide and further verified the applicability of SBAS-InSAR Technology in complex mountainous Landslide surveillance [12]. Zhang Pan et al. (2024) used SBAS-InSAR Technology with optical Remote Sensing Images and Unmanned Aerial Vehicle (UAV) photogrammetry to detect and identify active Landslides in the Maoergai Reservoir area. They identified 36 ancient reactivated Landslides and 29 newly formed Landslides [13]. In addition, Yang Chengsheng et al. (2024) conducted surveillance of the pre- and post-instability processes of the Baige Landslide in Tibet using SBAS-InSAR Technology. They successfully reconstructed the complete evolution of the Landslide event [14]. This demonstrates the broad application potential of SBAS-InSAR Technology in the identification and surveillance of Landslides. However, most current studies focus on the use of single-orbit data (either ascending or descending). This approach only provides one-dimensional line-of-sight deformation information and is insufficient to comprehensively reflect the three-dimensional Deformation Characteristics of Landslides [15,16]. In alpine canyon regions, steep terrain and varying slope aspects affect InSAR surveillance results from a single orbit because of satellite imaging geometry and local incidence angles. This makes it difficult to fully identify potential Landslide hazards [17,18]. Compared with using single-orbit data for Landslide surveillance, fusing ascending and descending InSAR data can overcome the limitations of a single orbit. By inverting the two-dimensional deformation field in the vertical and east–west directions, the fused data provide more comprehensive Landslide deformation information [19]. For example, a study in Dongchuan District, Yunnan, showed that fusing ascending and descending data can significantly improve the accuracy of Landslide hazard identification [20].

This study utilizes Sentinel-1A imagery from 89 ascending and 98 descending orbits to conduct wide-area deformation monitoring of the Xiluodu Reservoir's shoreline slopes during its water storage operation using SBAS-InSAR technology. By integrating orbital data from both ascending and descending phases, we reconstructed two-dimensional

surface displacement fields. We also systematically identified potential landslide hazard zones that have not yet undergone significant damage through visual interpretation of high-resolution remote sensing images. This work focuses on early-stage hazard detection and risk prediction during reservoir operations. It reveals spatiotemporal development patterns and progressive deformation trends of landslides in the reservoir area. The research findings provide critical scientific evidence and decision-making support for proactive geological disaster prevention in Xiluodu Reservoir, long-term safe operation of hydropower stations, and ecological conservation in surrounding areas.

2. Materials and Methods

2.1. Study Area

Xiluodu Hydropower Station is located in the downstream section of the Jinsha River, straddling the Sichuan–Yunnan border between Liangshan Yi Autonomous Prefecture (Sichuan Province) and Zhaotong City (Yunnan Province). As a major hydropower hub in the Jinsha River basin, its geographic location is illustrated in Figure 1. The reservoir lies on the eastern margin of the Hengduan Mountains (27°07′–28°21′ N, 102°42′–103°47′ E), characterized by deeply incised "V"-shaped gorges with elevations ranging from 2000 to 3500 m. Gorge depths reach approximately 1500 m, and slope gradients commonly exceed 30°, reflecting typical alpine canyon topography. The study area is predominantly covered by subtropical evergreen broad-leaved forests, dominated by Fagaceae and Lauraceae species, with dense understory shrubbery. Regionally, the stratigraphy consists mainly of interbedded Paleozoic carbonate rocks and shales. Intense tectonic activity has resulted in highly fractured rock masses with well-developed joint systems. Several active fault zones are present in the vicinity of the reservoir, contributing to complex geological conditions [21]. The climate is classified as a subtropical plateau monsoon type, with mean annual temperatures of 12–19.7 °C and annual precipitation of 800–1200 mm, concentrated primarily during the summer months. The reservoir's normal operating water level is 600 m, with an annual fluctuation range of 30–40 m during operation. These periodic water level variations significantly elevate seepage pressure within the bank slope rock mass. Coupled with intense rainfall infiltration during the rainy season, this process severely compromises the stability of reservoir bank materials, substantially increasing landslide susceptibility.

Numerous ancient landslides, formed during earlier geological periods, are widely distributed throughout the Xiluodu reservoir area. These landslides have generally attained a state of long-term stability through geological evolution, exhibiting considerable variation in size and scale. Some landslide bodies currently support settlements and infrastructure. Since reservoir impoundment, the toe zones of these ancient landslides have been subjected to repeated cycles of submergence and exposure due to periodic reservoir water level fluctuations. Under the synergistic influence of heavy rainfall infiltration and reservoir-induced hydrological loading, localized reactivation of these dormant landslides may be triggered. Such reactivation not only endangers existing infrastructure on the landslide masses but also carries the risk of catastrophic failure, river channel blockage, and the generation of impulse waves. Consequently, high-precision, full-coverage monitoring is critically needed to systematically elucidate the deformation mechanisms and dynamic evolution of landslides in the reservoir area. This effort is essential for ensuring safe reservoir operation and strengthening disaster risk prevention and mitigation strategies.

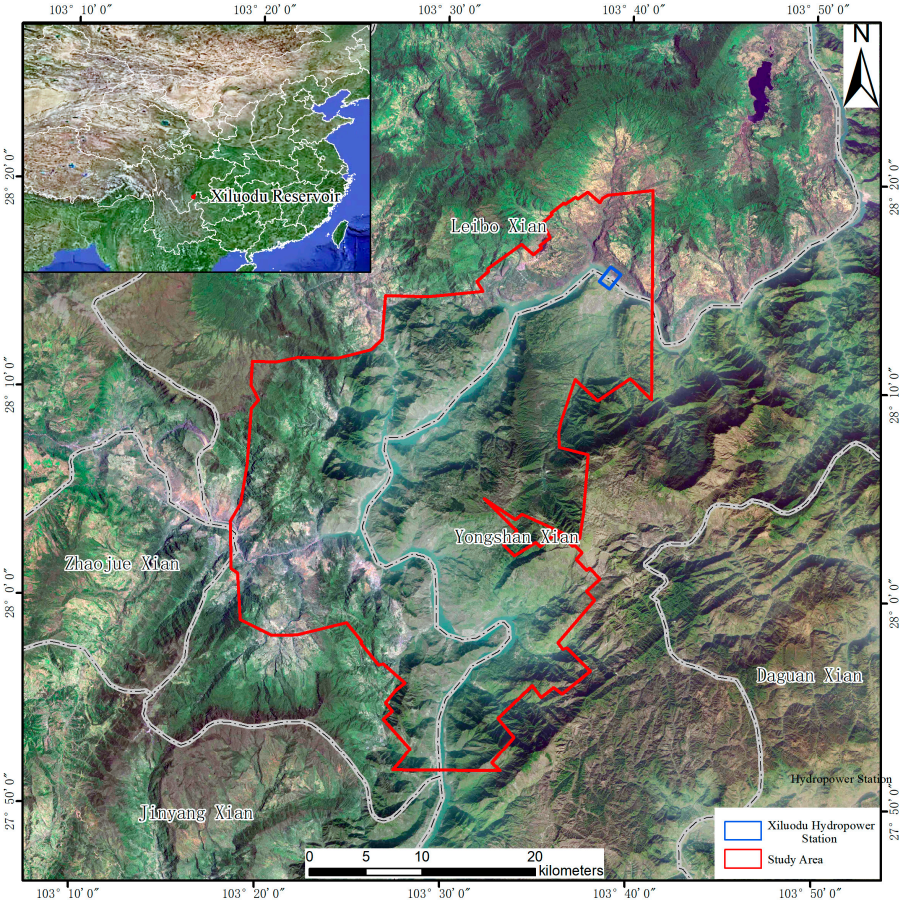


Figure 1. Study area scope.

2.2. Data Source

The Sentinel-1A data used in this study were acquired from the Copernicus Data Space Ecosystem of the European Space Agency (ESA), which provides free and open access to the Sentinel satellite data series. The dataset encompasses the Xiluodu Reservoir area and spans the period from January 2021 to May 2024, comprising 89 ascending and 98 descending orbit acquisitions. All scenes are Level-1 Single Look Complex (SLC) products acquired in Interferometric Wide (IW) swath mode, which is well-suited for surface deformation monitoring. Key acquisition parameters are summarized in Table 1. To enhance the accuracy of interferometric synthetic aperture radar (InSAR) processing, precise orbit ephemeris files (AUX_POEORB) were downloaded from the CDSE to ensure high-precision orbital information. Additionally, a 30-m resolution Shuttle Radar Topography Mission (SRTM) digital elevation model (DEM) was employed to remove topographic phase contributions and support interferometric processing. Precipitation data were obtained from the National Tibetan Plateau Data Center [22].

Table 1. Image parameters of Sentinel 1 ascending and descending orbits in the study area.

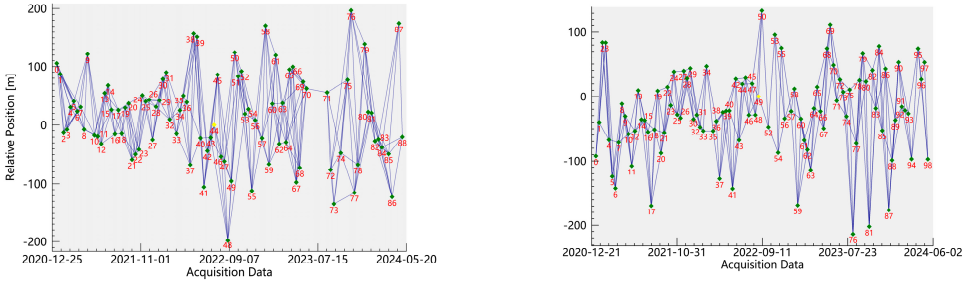
Orbit	Band	Resolution/m	Incidence Angle /(°)	Heading Angle /(°)	Polarization	Number of Acquisitions	Monitoring Period
Ascending Orbit	C	5 × 20	37.0	347.39	VV	89	10 January 2021–6 May 2024
Descending Orbit			37.2	192.62		98	5 January 2021–13 May 2024

2.3. Methods

2.3.1. The SBAS-InSAR Principles and Processing Flow

SBAS-InSAR is a time series analysis technique based on synthetic aperture radar interferometry, specifically designed to process SAR data subsets with relatively small spatial and temporal baselines. Its fundamental principle involves simply and efficiently combining all available small-baseline interferometric pairs, and then, based on the minimal deformation rate spatial extent criterion, using the singular value decomposition (SVD) method to obtain the deformation rate and its time series for coherent targets [23]. Compared with traditional InSAR methods, the core of the SBAS-InSAR approach lies in selecting image pairs that meet the small-baseline condition, effectively reducing the impact of atmospheric delay and decorrelation noise, and avoiding phase decorrelation issues caused by excessively large baselines. This results in greater adaptability in complex terrain and long time series monitoring, thereby improving the accuracy and reliability of deformation monitoring [24].

This study employs the SBAS-InSAR technique to process 89 ascending and 99 descending Sentinel-1A SLC images acquired between 2021 and 2024. The processing workflow includes data preprocessing, interferogram generation, phase unwrapping and detrending, deformation inversion, and geocoding. Due to the large spatial extent of the Xiluodu reservoir, adjacent scenes from the same orbit were mosaicked and cropped to ensure complete coverage of the study area. All images were coregistered to a common master with sub-pixel accuracy, and precise orbit data were applied to minimize geometric distortions. Interferograms were generated using a 4:1 multilooking ratio (range × azimuth) to balance spatial resolution and signal-to-noise ratio, while suppressing speckle noise. A short temporal baseline approach was adopted, with a maximum temporal baseline of 36 days and a spatial baseline threshold of 5% of the critical baseline. This threshold was selected to mitigate temporal decorrelation caused by rapid vegetation growth during the rainy season (May–October), ensuring coherence values above 0.7 in most bedrock and stable surface areas. A total of 583 high-quality interferometric pairs (274 ascending, 309 descending) were formed, as shown in Figure 2. The topographic phase was removed using the 30 m SRTM DEM Before unwrapping, Goldstein filtering was applied to reduce phase noise, followed by phase unwrapping using the Minimum Cost Flow (MCF) algorithm. Time-series deformation was inverted using Singular Value Decomposition (SVD), incorporating a hybrid PS-SBAS approach that combines permanent scatterers (PS) and distributed scatterers (DS) to improve spatial coverage and reliability [25]. To correct for atmospheric artifacts—particularly stratified tropospheric delays in mountainous terrain—we applied tropospheric delay corrections from the Generic Atmospheric Correction Online Service (GACOS), which integrates ERA5 meteorological reanalysis with InSAR geometry [26]. Finally, the deformation results were geocoded to the WGS84 coordinate system, generating both deformation velocity maps and time series for spatial analysis.



(**a**) (**b**)

Figure 2. Interferometric pairs: (**a**) temporal–spatial baseline plot for the ascending orbit; (**b**) temporal–spatial baseline plot for the descending orbit.

2.3.2. Two-Dimensional Deformation Decomposition

SBAS-InSAR Technology can obtain one-dimensional deformation information along the radar's line of sight (LOS) from single-orbit radar images. However, actual Landslide deformation is inherently three-dimensional. Therefore, by integrating data from multiple orbits, a two-dimensional deformation field can be derived [27]. Due to the side-looking nature of radar imaging, LOS deformation can be decomposed into a linear combination of vertical (V), east–west (E), and north–south (N) components. However, since ascending and descending orbits satellite tracks are approximately aligned in the north–south direction, radar sensitivity to north–south deformation is extremely low and can thus be neglected. This simplifies the decomposition to a combination of only vertical and east–west components [14,28]. The expression for this is

$$d_{\mathrm{LOS}} = d_V \cdot \cos\theta - d_E \cdot \sin\theta \cdot \cos\alpha \tag{1}$$

By combining ascending and descending data, two independent observation equations can be constructed:

$$\begin{cases} d_{\mathrm{LOS}}^{\mathrm{As}} = d_V \cdot \cos\theta_{\mathrm{As}} - d_E \cdot \sin\theta_{\mathrm{As}} \cdot \cos\alpha_{\mathrm{As}} \\ d_{\mathrm{LOS}}^{\mathrm{De}} = d_V \cdot \cos\theta_{\mathrm{De}} - d_E \cdot \sin\theta_{\mathrm{De}} \cdot \cos\alpha_{\mathrm{De}} \end{cases} \tag{2}$$

In the equation, $d_{\mathrm{LOS}}^{\mathrm{As}}$ and $d_{\mathrm{LOS}}^{\mathrm{De}}$ represent the deformation in the LOS direction for ascending and descending orbits, respectively; α_{As} and α_{De} denote the flight direction azimuth angles for ascending and descending orbits; θ_{As} and θ_{De} indicate the incidence angles of the radar line-of-sight for ascending and descending orbits. The system of equations contains only two unknowns, d_V and d_E, which can be solved using the least-squares method to derive the vertical and east–west deformation rates, thereby achieving the separation of the two-dimensional deformation field.

3. Results

3.1. Analysis of the LOS Deformation Results

In this study, the Small Baseline Subset Interferometric Synthetic Aperture Radar (SBAS-InSAR) technique was employed to monitor surface deformation in the Xiluodu Reservoir area. The LOS deformation rates derived from both ascending and descending satellite orbits between January 2021 and May 2024 are presented in Figure 3. Positive values denote motion toward the satellite, whereas negative values indicate displacement away from it. Overall, the deformation patterns obtained from ascending and descending orbits demonstrate strong spatial consistency. The LOS deformation rates range from −133.6 to +108.4 mm/year in the ascending orbit and from −145.3 to +114.6 mm/year in the descending orbit. Most residential areas surrounding the Xiluodu Hydropower Station exhibit minimal deformation, indicating a stable condition, whereas pronounced deformation is predominantly localized along the reservoir banks.

There is a discrepancy in the number of identified Landslide deformation zones based on single-orbit surveillance. In the ascending orbit deformation surveillance results shown in Figure 3, a total of 7 Significant Deformation Zones were identified, while 9 Significant Deformation Zones were identified in the descending orbit results. In addition, data loss occurred due to layover effects on certain slopes on both sides of the reservoir area in the ascending orbit, whereas the descending orbit provided better coverage on the eastern bank of the reservoir area, identifying more deformation zones than the ascending orbit. This highlights the limitations of single-orbit surveillance. Particularly in mountainous areas with significant topographic relief, relying solely on deformation results from a single orbit may lead to missed or incorrect identification of potential hazard zones. Therefore,

integrating ascending and descending orbit deformation fields to perform two-dimensional (2D) displacement decomposition can significantly enhance spatial coverage and improve the reliability of landslide hazard identification in complex terrain.

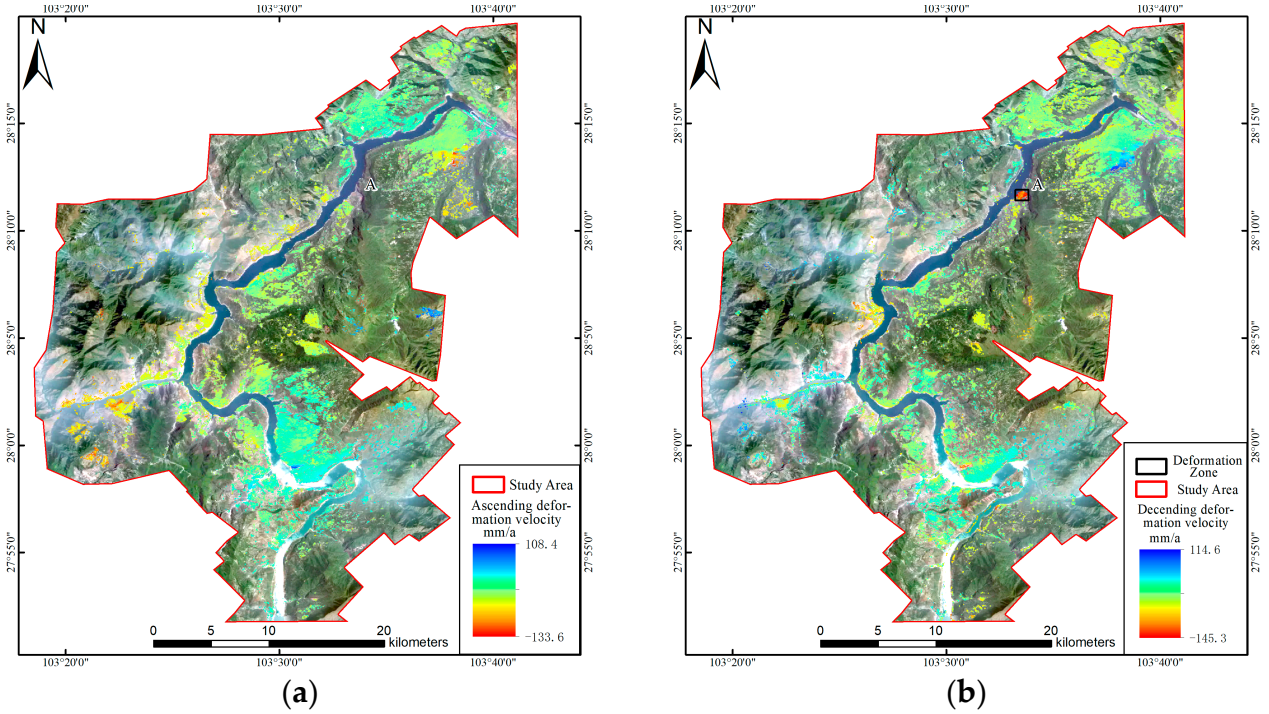


Figure 3. (**a**) Deformation velocity in the LOS direction for the ascending orbit. (**b**) Deformation velocity in the LOS direction for the descending orbit.

3.2. Analysis of Two-Dimensional Deformation Results

The annual mean deformation velocities derived from ascending and descending orbit data were decomposed using a two-dimensional (2D) deformation decomposition model to retrieve vertical and east–west displacement components across the study area. The results are presented in Figure 4, where positive values denote vertical uplift and eastward motion, respectively. As shown in Figure 4, the magnitudes of the decomposed vertical and horizontal deformation velocities differ from those observed in the LOS direction. The vertical velocity ranges from −113.8 to +65.8 mm/year, while the east–west horizontal velocity varies between −105.3 and +163.5 mm/year. Applying a consistent deformation velocity threshold, 10 and 12 distinct deformation zones were identified in the vertical and east–west components, respectively, based on the integrated 2D results. Owing to the influence of multiple factors—including the SAR satellite's incidence and azimuth angles, local terrain slope and aspect, and the geometric projection between the actual displacement vector and the radar line-of-sight direction—certain deformation zones exhibit pronounced motion in only one of the two orbital geometries. For instance, deformation zone A, clearly detected in the descending orbit, was not observable in the ascending orbit; consequently, no 2D decomposition result could be derived for this location. The number of deformation zones identified from the combined ascending and descending data is higher than that from either orbit alone, indicating that multi-orbit integration enhances the coverage and reliability of deformation detection. In addition, in areas where both ascending and descending data exhibit significant LOS deformation (e.g., deformation zone B), the combined results show high consistency, confirming the authenticity of the deformation signals in these regions.

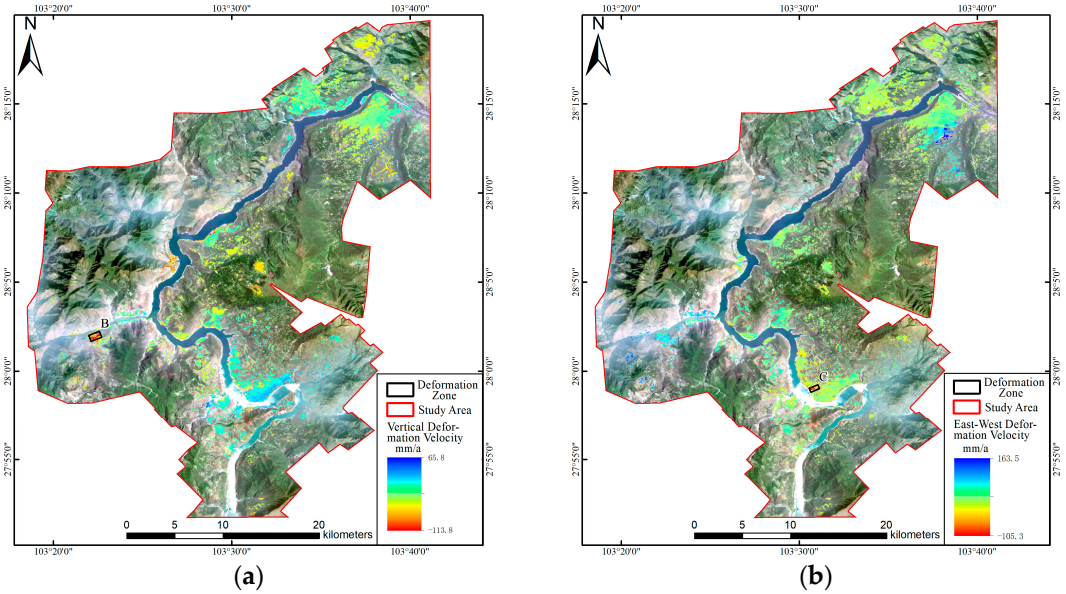


Figure 4. (**a**) Vertical deformation velocity (**b**) East–West deformation velocity.

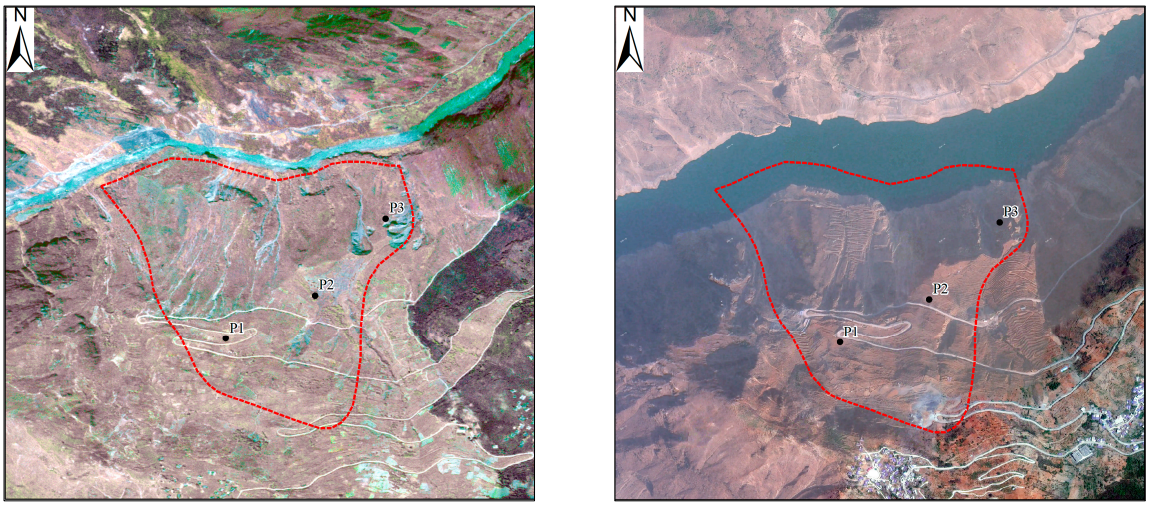
The primary advantage of fusing ascending and descending orbit data lies in its ability to partially resolve one-dimensional LOS observations into two-dimensional displacement components in the vertical and east–west directions, thereby enabling a preliminary identification of dominant deformation mechanisms. Taking deformation zone B as an example, LOS observations from the ascending orbit suggest subsidence, whereas those from the descending orbit indicate uplift. However, the combined observation results clearly reveal significant vertical subsidence (−102.9 mm/a), while the horizontal displacement in the east–west direction (43.9 mm/a) is relatively small compared with the vertical component. In contrast, deformation zone C exhibits markedly different behavior: vertical deformation is negligible, but consistent and significant westward motion is observed in the east–west component at a rate of −100.5 mm/year. This pattern—characterized by large horizontal displacement and minimal vertical movement—is a typical InSAR signature of potential landslides or slope creep, as landslide motion is generally governed by shear displacement along the slip surface, with only limited vertical subsidence. Single-orbit LOS observations in such settings may either underestimate the true deformation magnitude or misinterpret the kinematic direction; in contrast, 2D decomposition based on fused ascending and descending orbit data clearly delineates the dominant motion pattern.

3.3. Characterization of Typical Deformation Areas

Based on the fused ascending and descending orbit results presented in Section 3.2, two deformation zones exhibiting distinct dominant motion patterns were identified in the study area. Accordingly, this section focuses on two representative regions: deformation zone B (the Mixiluo landslide), characterized by dominant vertical displacement, and deformation zone C (the Huanghua landslide), dominated by horizontal movement. A detailed analysis of their spatiotemporal evolution, formation mechanisms, and potential hazards is conducted by integrating multi-source data, including remote sensing imagery, topography, geological maps, and reservoir water level records.

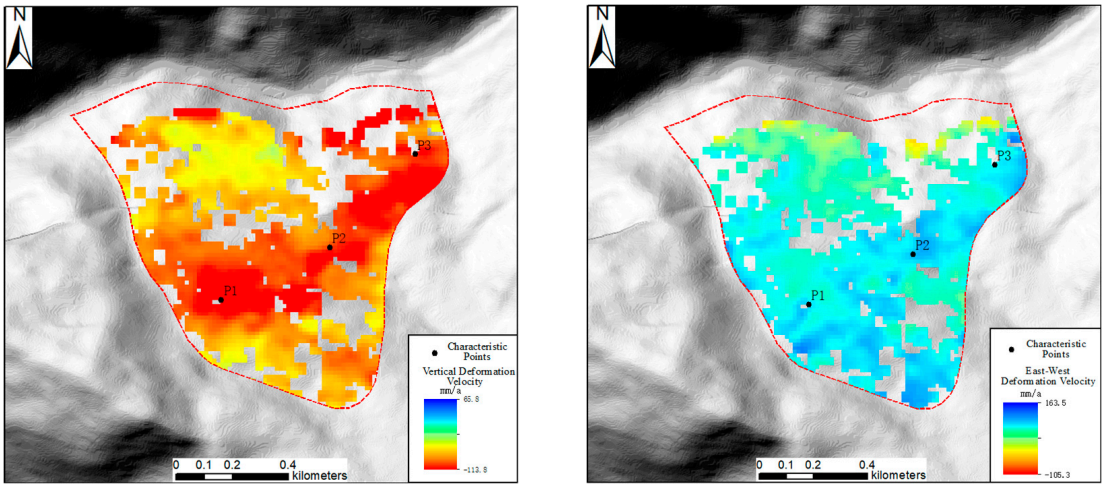
The Mixiluo Landslide is located on the bank slope of a tributary on the left bank of the Jinsha River in Leibo County, Liangshan Yi Autonomous Prefecture, Sichuan Province. The elevation of the landslide area ranges from 480 m to 1180 m. The stratigraphy mainly consists of gray-black and gray-green argillaceous quartz siltstone interbedded with fine sandstone and marl. The rock layers have a steep dip angle, and the dip direction is

nearly perpendicular to the slope direction, forming an unfavorable reverse slope structure. Figure 5 shows the Remote Sensing Images of the landslide during different periods before and after reservoir impoundment, with all image data sourced from Jilin-1. It can be observed that a small number of residential areas are distributed above the rear edge of the landslide, and a winding mountain road passes through the central part. Comparing the images from the two periods, due to reservoir filling, part of the toe of the slope has been completely submerged. To further analyze the Deformation Characteristics of the Mixiluo Landslide, based on the deformation results (Figure 6), one typical feature point (P1, P2, P3) was selected at the front edge, central part, and rear edge of the landslide, respectively.



(**a**) (**b**)

Figure 5. Remote sensing images of Mixiluo Landslide in 2013 (**a**) and 2023 (**b**).



(**a**) (**b**)

Figure 6. Annual mean deformation velocity maps of the Vertical (**a**) and East–West (**b**) components for Mixiluo Landslide.

The cumulative displacement time series for these points were extracted and compared with concurrent rainfall records, as shown in Figure 7. Although precise reservoir water level data were unavailable, comparison with the water level variation pattern reported in [10] suggests a positive correlation between reservoir level fluctuations and rainfall, with the water level response exhibiting a slight temporal lag relative to precipitation. Consequently, the rainy season is typically accompanied by a rise in reservoir water level. Due to the unavailability of official reservoir water level records, water level data were not

included in any quantitative analysis. In discussing deformation mechanisms, reservoir level fluctuations are mentioned only as an indirect proxy for rainfall, based on prior evidence that water level and precipitation are highly synchronized at this site. This reference does not imply a quantitative or causal relationship between water level and deformation. Future studies incorporating high-quality in situ water level measurements would enable the disentanglement of the individual effects of rainfall infiltration and reservoir drawdown/uplift on landslide deformation. Comparative analysis of the three characteristic points indicates that the overall deformation pattern of the landslide is dominated by vertical subsidence, with relatively minor horizontal displacement. During the non-rainy season, all parts of the landslide exhibit approximately uniform and steady downward movement. In contrast, during the rainy season—particularly during periods of intense rainfall—the deformation rate increases markedly, displaying a typical "step-like" acceleration pattern. During the rainy seasons of May and July–September in 2021 and 2022, both the front and rear edges of the landslide experienced pronounced acceleration in deformation, whereas the changes during the 2023 rainy season were relatively minor. The rear edge of the landslide is characterized primarily by significant vertical subsidence with minimal horizontal displacement. In contrast, the front edge exhibits not only vertical subsidence but also notable eastward horizontal displacement, indicating a compound shear–subsidence deformation mechanism directed toward the Jinsha River.

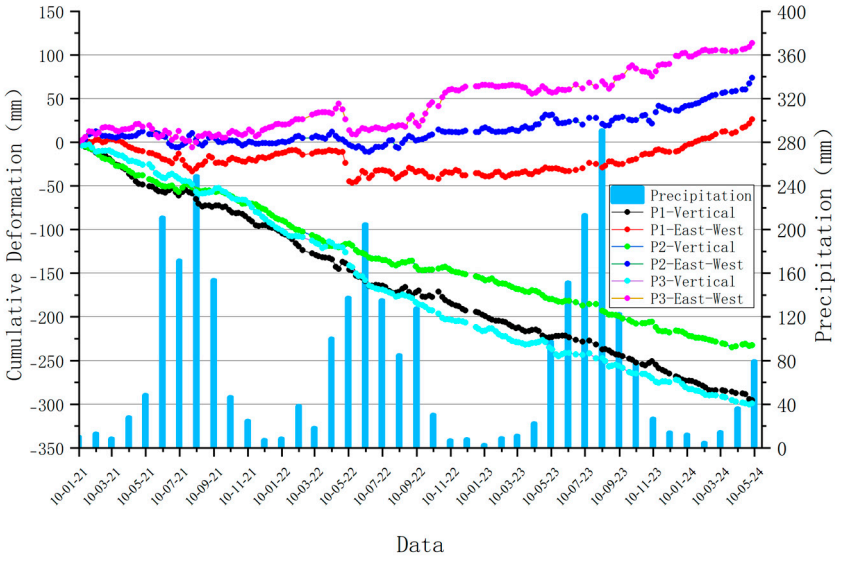
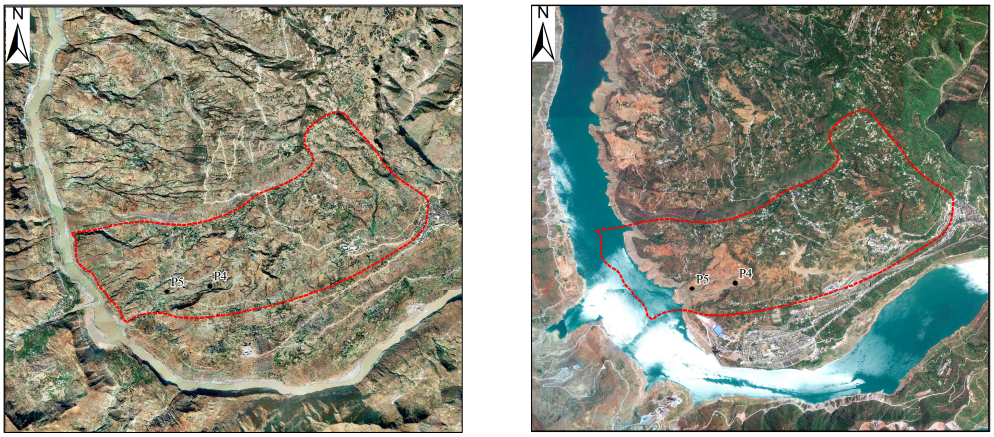


Figure 7. Deformation time series of feature points and monthly mean precipitation.

Consequently, the deformation of the Mixiluo landslide is primarily driven by the combined effects of rainfall infiltration and fluvial scouring from tributaries of the Jinsha River. Rainfall infiltration increases the self-weight of the landslide mass and softens the weak interlayers within the argillaceous siltstone. Coupled with the soaking–softening effect and hydrodynamic pressure induced by reservoir water level fluctuations, these processes collectively reduce the shear strength of the sliding zone, thereby triggering accelerated deformation. The contrasting deformation behavior between the front and rear edges suggests that the landslide is currently undergoing a progressive traction-type failure process, necessitating continuous monitoring of its stability.

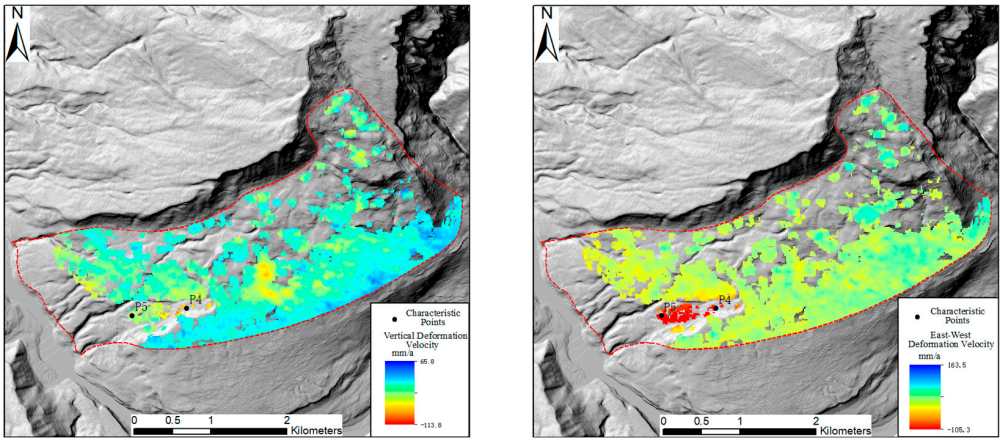
The Huanghua landslide is located in Huanghua Township, Yongshan County, Yunnan Province, on the right bank of the Jinsha River. The rock strata exhibit a relatively low dip angle, with the dip direction generally consistent with the slope aspect. The deformed zone primarily consists of medium- to thick-bedded siltstone and mudstone, whereas the central and rear portions are predominantly composed of gray, medium- to thick-bedded limestone,

exhibiting considerable variation in stratal attitude. Figures 8 and 9 present the remote sensing imagery and deformation results, respectively. Following reservoir impoundment, part of the slope toe has been fully submerged. Spatially, deformation is concentrated in the toe area adjacent to the Jinsha River shoreline. Vertical displacement is negligible, while horizontal creep is observed in the east–west direction, trending westward toward the river channel. In contrast, the central and rear parts of the landslide show minimal deformation and remain generally stable. Therefore, one characteristic point was selected at the landslide toe and another at the central-rear part (P4, P5) for analysis, as shown in Figure 10. During the period from 2021 to 2024, the cumulative vertical displacement of the two feature points remained within 50 mm. In the horizontal direction, they exhibited a nearly uniform westward movement, with a slight increase in velocity observed during the rainy season from June to October each year. The cumulative displacement at the toe of the slope (P5) was significantly greater than that at the middle-rear section (P4). The lithology of the strongly deformed toe area mainly consists of Ordovician–Silurian siltstone and mud shale. These rock types are prone to softening upon water exposure and have poor weathering resistance. Under the scouring action of the Jinsha River water, they are easily eroded, leading to localized collapses and slides. Therefore, it can be inferred that the high annual rainfall and the long-term lateral erosion by the Jinsha River are the primary factors contributing to the reduction in sliding resistance and the occurrence of localized instability in this area.



(**a**) (**b**)

Figure 8. Remote sensing images of Huanghua Landslide in 2013 (**a**) and 2023 (**b**).



(**a**) (**b**)

Figure 9. Annual mean deformation velocity maps of the Vertical (**a**) and East–West (**b**) components for Huanghua Landslide.

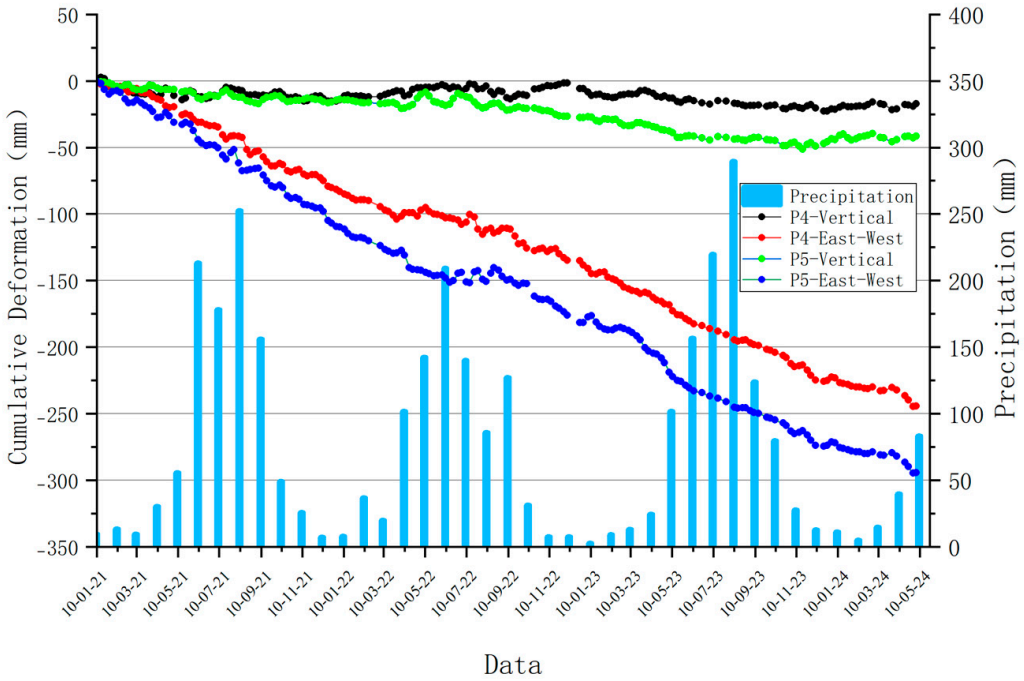


Figure 10. Deformation time series of feature points and monthly mean precipitation.

To enhance the reliability of our findings, we compared our results with those from studies conducted in the Baihetan Reservoir area, which is also located in the Jinsha River basin. In [29], the Xiaxiaomidi landslide was identified as the most actively deforming slope in the Baihetan reservoir region, with a maximum cumulative displacement of –317.4 mm. This landslide exhibits a retrogressive (toe-driven) failure pattern, likely caused by toppling deformation at the toe due to reservoir water level fluctuations, leading to gradual creep [29]. In [30], the Dawanzi landslide was interpreted as a translational (push-type) slide primarily triggered by the combined effects of intense rainfall and reservoir-induced water level rise. These comparative cases from the Baihetan reservoir support our interpretation that reservoir-induced hydrological changes (e.g., water level fluctuations) and rainfall act as key drivers of different landslide kinematic modes in canyon-type reservoir settings. The consistency in deformation mechanisms across adjacent reservoirs strengthens the validity of our conclusions regarding the hydro-mechanical triggers of slope instability in the Xiluodu Reservoir area.

Meanwhile, to quantitatively assess the relationship between rainfall and deformation in future analyses, we employ Pearson's correlation coefficient, which reveals distinct hydro-mechanical responses at the two study sites. At the Huanghua landslide, a strong and highly significant positive correlation is observed ($r = 0.538$, $p = 0.0007$), indicating that monthly deformation is closely and directly linked to concurrent rainfall, likely reflecting a rapid infiltration response in a shallow or pre-conditioned slope. In contrast, the Mixiluo landslide exhibits a weaker but still statistically significant correlation ($r = 0.358$, $p = 0.031$), suggesting that rainfall plays a more limited or indirect role in driving deformation—possibly due to deeper slip mechanisms, buffering by vegetation or soil layers, or the influence of additional controlling factors such as reservoir water level fluctuations or antecedent moisture conditions. These differences highlight the site-specific nature of landslide hydrological sensitivity and underscore the need for localized monitoring and modeling approaches.

4. Discussion

Based on long-term InSAR technology from the combined ascending and descending orbits, this study conducts deformation surveillance of the Xiluodu Reservoir area landslide using ascending and descending track Sentinel 1A data from January 2021 to May 2024. The spatial distribution of landslide deformation in the study area is obtained, and a two-dimensional deformation field is derived by separating the LOS deformation results from ascending and descending tracks.

(1) Compared to single-orbit monitoring approaches commonly used in alpine canyon regions, the integration of ascending and descending InSAR tracks significantly enhances both spatial coverage and monitoring reliability by identifying a greater number of deforming areas and accurately separating deformation components in different line-of-sight directions. This provides robust data support for precisely characterizing landslide kinematics and understanding their underlying mechanisms. Furthermore, when combined with visual interpretation of remote sensing imagery, this approach enables early warning of potential landslide hazards, offering proactive measures for disaster prevention and mitigation.

(2) Surveillance data from two selected typical deformation zones indicate that reservoir water level fluctuation is one of the primary triggering factors for landslide development and deformation in the reservoir area. In future work, integrating in situ monitoring data with numerical simulations—such as hydro-mechanical coupled models—would enable more rigorous quantitative analysis of landslide deformation mechanisms. Furthermore, incorporating advanced machine learning approaches, such as deep learning algorithms, could enhance the predictive capability of landslide behavior under varying reservoir operation schedules and rainfall scenarios.

(3) The SBAS-InSAR technology has successfully reconstructed the spatiotemporal evolution of landslide deformation in deep canyon reservoirs, demonstrating its capability to detect deformation risks early, quantify deformation rates, and analyze triggering factors in large-scale, complex environments. This provides scientific evidence and technical solutions for ensuring the safe operation of reservoirs with similar geological conditions.

Author Contributions: Writing, Y.L.; Conceptualization, F.D. and X.W.; methodology, F.D., X.W. and Y.L.; software, Y.L.; validation, X.W. and Y.L.; investigation, X.W., Y.L. and Z.W.; resources, F.D., X.W., Y.L. and Z.W.; formal analysis, X.W. and Y.L.; data curation, X.W. and Y.L.; writing—original draft preparation, Y.L.; writing—review and editing, X.W. All authors have read and agreed to the published version of the manuscript.

Funding: This research received no external funding.

Data Availability Statement: Data will be made available upon request.

Acknowledgments: I am deeply grateful to my supervisor, Xiaodong Wang, for his guidance and support throughout this research, and I would also like to extend my sincere thanks to the Copernicus Data Space Ecosystem and the National Tibetan Plateau/Third Pole Environment Data Center (http://data.tpdc.ac.cn, accessed on 15 August 2025).

Conflicts of Interest: The authors declare no conflicts of interest.

References

1. Lu, Y.X.; Xiao, J.Z.; Xu, C.; Xie, Q.Z.; Yuan, H. Deformation mechanism and stability analysis of landslides under the influence of reservoir impoundment and construction activities. *J. Eng. Geol.* **2014**, *22*, 386–395.
2. Tang, F.J.; Qi, S.W.; Guo, S.F.; Zou, Y.; Li, Y.; Lu, X.; Hou, X. Spatiotemporal distribution Patterns and susceptibility of reservoir-induced landslides in the Xiluodu reservoir area of the Jinsha River. *J. Eng. Geol.* **2022**, *30*, 609–620.

3. Zeng, Y.H.; Zheng, D.; Wu, Z.L.; Li, Q.F.; Pan, Y.Y.; Liu, J.F. Study on the Reactivation Mechanism of Typical Reservoir Bank Deposits under High Water Level and Large Amplitude Fluctuations. *Yangtze River* **2025**, 1–13. Available online: https://link.cnki.net/urlid/42.1202.TV.20250414.2206.002 (accessed on 30 September 2025).
4. Zhang, E.; Li, Y.; Li, S.; Li, M.; Zhang, X. Physical model experimental study on the deformation mechanism of Baijiabao landslide in the Three Gorges Reservoir Area. *Saf. Environ. Eng.* **2025**, *32*, 218–230.
5. Yi, Q.L.; Wang, B.; Deng, M.L.; Dong, Q.; Liu, K.X.; Zhang, J.X.; Lai, X.M. Deformation characteristics and mechanism of landslides induced by rainfall raising groundwater level in the Three Gorges Reservoir Area. *J. China Three Gorges Univ. (Nat. Sci.)* **2023**, *45*, 105–115.
6. Xu, D.; Wang, T.; Da, S.; Yang, A.P.; Li, J.S.; Zhu, J.D. Application of SBAS-InSAR technology in the deformation monitoring of a super-large landslide: A case study of Pangcun landslide in Tibet Autonomous Region. *Sci. Technol. Eng.* **2021**, *21*, 14927–14935.
7. Dong, Y.J.; Zuo, X.Q.; Li, Y.F.; Zhang, J.M.; Chen, K. Deformation monitoring and landslide identification in a reservoir area of a Southwest China power station based on DS-InSAR. *Remote Sens. Inf.* **2024**, *39*, 104–111.
8. Li, S.; Xu, W.; Li, Z. Review of the SBAS InSAR Time-series algorithms, applications, and challenges. *Geod. Geodyn.* **2022**, *13*, 114–126. [CrossRef]
9. Tao, C.; Zhang, Y.; Ren, S. Research progress on the application of InSAR technology in landslide identification and monitoring. *Geol. China* **2025**, *52*, 513–526.
10. Yang, B.; Zhao, R.Z.; Wang, H.B.; Li, X.G.; Lü, Z.; Zhao, Y.; Wang, M.Y. Early identification and dynamic monitoring of geological hazards by remote sensing technology: A case study of the Changbo Township to Yangla Township section. *Sci. Technol. Eng.* **2024**, *24*, 1823–1836.
11. Khan, B.A.; Zhao, C.; Kakar, N.; Chen, X. SBAS-InSAR Monitoring of Landslides and Glaciers Along the Karakoram Highway Between China and Pakistan. *Remote Sens.* **2025**, *17*, 605. [CrossRef]
12. Feng, W.; Dun, J.; Yi, X.; Zhang, G.Q. Deformation analysis of the Woda Village giant ancient landslide in Jinsha River Basin based on SBAS-InSAR technology. *J. Eng. Geol.* **2020**, *28*, 384–393.
13. Zhang, P.; Li, W.L.; Lu, H.Y.; Zhou, S.; Li, W.M.; Xu, S.M. Response relationship between deformation characteristics of active landslides in reservoir area and reservoir water level variation based on SBAS-InSAR: A case study of Maoergai Hydropower Station in Heishui County, Sichuan Province. *Sci. Technol. Eng.* **2024**, *24*, 11991–12002.
14. Yang, C.S.; Wei, C.R.; Wei, Y.J.; Li, Z.F.; Ding, H.L. Whole-process deformation monitoring before and after the instability of the Baige landslide in Tibet based on multi-source remote sensing images. *Remote Sens. Nat. Resour.* **2025**, *37*, 203–211.
15. Li, Z.H.; Chen, B.; Liu, Y.P.; Peng, J.B.; Xu, Q.; Jiang, L.W.; Du, J.T.; Song, C.; Ding, M.T.; Zhu, W. Long-term 3D deformation monitoring and risk assessment of the Guba landslide on the Tibetan Plateau. *Sci. China Earth Sci.* **2025**, *55*, 3421–3437. [CrossRef]
16. Shi, G.L.; Chen, Q.; Liu, X.W.; Yang, Y.H.; Xu, Q.; Zhao, J. Monitoring the slope-oriented deformation velocity field of Taoping ancient landslide using ascending and descending Sentinel-1A data. *J. Eng. Geol.* **2022**, *30*, 1350–1361.
17. Bao, X.; Zhang, R.; Liu, A.; Wang, T.; Xiang, W.; Liu, G.X. Potential landslide identification of Jinsha River landslide group by joint time-series InSAR of ascending and descending orbits. *J. Beijing Inst. Technol.* **2023**, *43*, 1135–1145.
18. Li, Z.R.; Sha, Y.L.; Xin, R.F.; Zhang, X.; Sui, J.; Sun, H. Early identification and characteristic analysis of landslide hazards in Tongren City, Qinghai Province based on time-series InSAR. *Sci. Technol. Eng.* **2023**, *23*, 15158–15170.
19. Dun, J.W.; Feng, W.K.; Yi, X.Y.; Zhang, G.Q.; Wu, M.T. Early identification of active landslides by InSAR before impoundment in Baihetan Reservoir Area: A case study from Hukou Town to Xiangbiling section. *J. Eng. Geol.* **2023**, *31*, 479–492.
20. Liu, P.Y.; He, S.S.; Wang, P.S.; Sun, L. Early identification of landslide hazards in Southwest mountainous areas based on ascending and descending Sentinel-1A SBAS-InSAR. *J. Geod. Geodyn.* **2022**, *42*, 892–897.
21. Liang, Y.; Yan, L.; Su, P.D.; Qiu, P.; Long, W.; Wang, Y.L. Deformation characteristics and formation mechanism of thehekou landslide in the Xiluodu reservoir area. *Sci. Technol. Eng.* **2021**, *21*, 14500–14507.
22. Zhu, Z.; Gan, S.; Yuan, X.; Zhang, J.; Wang, R.; Zhang, X. Identification of landslide hazards in Dongchuan District by integrating ascending and descending InSAR data. *Prog. Geophys.* **2023**, *38*, 137–146.
23. Peng, S. 1-km monthly precipitation dataset for China (1901–2024). *Earth Syst. Sci. Data* **2019**, *11*, 1931–1946. [CrossRef]
24. Guo, J.; Xi, W.; Yang, Z.; Shi, Z.; Huang, G.; Yang, Z.; Yang, D. Landslide hazard susceptibility evaluation based on SBAS-InSAR technology and SSA-BP neural network algorithm: A case study of Baihetan Reservoir Area. *J. Mt. Sci.* **2024**, *21*, 952–972. [CrossRef]
25. Li, X.Y.; Yin, K.L.; Liang, X.; Xie, X.X.; Liao, Y.X.; Wang, N.N.; Yin, H. Time-series deformation characteristics analysis of the Outang landslide hazard based on PS-SBAS-InSAR. *Saf. Environ. Eng.* **2025**, *32*, 216–229.
26. Li, M.J.; Sun, J.B.; Xue, L.; Shen, Z.K. Monitoring land surface deformation in the North China Plain using wide-area InSAR time-series analysis. *Acta Sci. Nat. Univ. Pekin.* **2023**, *59*, 934–944.
27. Li, L.J.; Yao, X.; Zhou, Z.K.; Wang, D.F. Suitability evaluation of Sentinel-1 data for InSAR monitoring of deformation slopes in reservoir areas of southwestern mountainous regions: A case study of Xiluodu Reservoir. *J. Geomech.* **2022**, *28*, 281–293.

28. Yang, L.; Luo, H.H.; Jiang, P.; Li, L.Z.; Fan, J.Y.; Liao, H.S.; An, R.H.; Tu, J.; Chen, J.; Yan, B.; et al. Monitoring and application of reservoir bank landslides in large hydropower stations using time-series InSAR technology. *Geospat. Inf.* **2025**, *23*, 13–17.
29. Wei, C.H.; Li, W.L.; Wu, Z.L.; Zhou, S.S.; Wang, X.; Li, X.Q.; Li, Y.S. Identification of active landslides and analysis of deformation influencing factors in the Baihetan reservoir area. *Bull. Geol. Sci. Technol.* **2025**, *44*, 62–77.
30. Yang, Z.R.; Xi, W.F.; Shi, Z.T.; Xiao, B.; Zhou, D.Y. Deformation analysis of potential reservoir bank landslides at the Baihetan Hydropower Station based on SBAS-InSAR. *Chin. J. Geol. Hazard Control* **2022**, *33*, 83–92.

Disclaimer/Publisher's Note: The statements, opinions and data contained in all publications are solely those of the individual author(s) and contributor(s) and not of MDPI and/or the editor(s). MDPI and/or the editor(s) disclaim responsibility for any injury to people or property resulting from any ideas, methods, instructions or products referred to in the content.